Chapter 1
Linear and Nonlinear Response of a Continuous-Interface BARC: FEA Prediction and Test

Sean Magoffin, Brooklyn Andrus, Matthew S. Allen, and Raymond Joshua

Abstract This paper presents the results of finite element modeling and linear and nonlinear testing of a BARC structure with a continuous interface (as opposed to the split-interface BARC). Before the actual hardware was constructed, blueprints were used to create a FEM in which the bolts were modeled in detail, including contact at the interfaces due the expected preload based on the bolt torque specs. This model was used to predict the linearized natural frequencies, to infer which modes might exhibit nonlinearity, and then quasi-static modal analysis was used to predict the amplitude dependent natural frequency and damping for the modes that were expected to exhibit the strongest nonlinearity. Once the FEM predictions were mostly complete, a BARC was constructed based on the blueprints and tests were performed to measure its linear modes and characterize those modes that exhibit nonlinear behavior. The linear modes measured in test are compared to those computed from the FEM about the preloaded state. Additionally, for those modes where significant nonlinearity was observed, quasi-static modal analysis (QSMA) was used to predict their amplitude dependent natural frequencies and damping ratios.

Keywords BARC · Quasi-static modal analysis · Nonlinearities · FEA

Introduction

The Box Assembly with Removable Component (BARC) structure was created in 2017 to provide a common benchmark structure to evaluate dynamic environment testing methods [1]. State of the art environmental testing methods do not consider nonlinearity, although one could argue that they seek to capture it by testing the component of interest at high enough levels that any nonlinearities would be observed. In any event, while many studies have tested and modeled the BARC over the past decade, very few focused on its nonlinear behavior. On the other hand, because the removable component consists of three parts bolted together, it can behave nonlinearly and experimental campaigns have noted this since it was introduced. This work presents a first effort to characterize the nonlinear behavior of the continuous-interface BARC structure, both experimentally and using nonlinear finite element simulations.

This study is a complement to the various studies that have used experimental modal analysis to extract the linear modes of the BARC and compared those with modes from finite element models. For example, Alvis and Schoenherr [2] used the BARC to perform a detailed study on the best practices for modeling bolted interfaces. Their study, as with others,

Honeywell Federal Manufacturing & Technologies, LLC operates the Kansas City National Security Campus for the United States Department of Energy / National Nuclear Security Administration under Contract Number DE-NA0002839. UUR – NSC-614-6620

Sean Magoffin · Brooklyn Andrus
Undergraduate Students, Brigham Young University, Department of Mechanical Engineering
e-mail: sm996@byu.edu; brookand@byu.edu

Matthew S. Allen
Professor, Brigham Young University, Department of Mechanical Engineering
e-mail: matt.allen@byu.edu

Raymond Joshua
Sr. Mechanical Engineer, Advanced Development Domain (ADD), Kansas City National Security Campus
e-mail: rjoshua@kcnsc.doe.gov

Ludovic Renson et al. (eds.), *Nonlinear Structures & Systems, Vol. 1*, Conference Proceedings of the Society for Experimental Mechanics Series, https://doi.org/10.13052/97887-438-0146-7_1

[3][4][5][6] focused on the low amplitude, linearized behavior. Several studies have had good success in creating finite element models that correlated very well with measurements of the natural frequencies and mode shapes of the BARC, although most have noted that care had to be taken in modeling the bolted connections appropriately. The authors found very few studies that quantified the nonlinear behavior of the BARC. Takeshita's thesis [7] and some precursor papers did explore this somewhat, in particular the randomly excited response of the BARC to a base input. No other detailed studies were found before this paper had to be submitted. In this work the BARC is tested and simulated in free-free conditions. Note also that this study focuses on the continuous-interface BARC, while many prior studies have focused on the split-interface BARC.

In undertaking this study, the authors began with blueprints of the BARC structure, and the finite element models were created from those before any hardware had been machined. The authors did have the benefit of comparing their results to other papers that had also modeled this structure, but other than that the predictions were blind in that the linear and nonlinear testing was not performed until after the finite element models had been created and debugged. The FEM included a simplified, three-dimensional model of the bolts, which were preloaded based on the torque specified in the assembly drawings. The FEM was created in Abaqus, which solved the nonlinear contact problem to obtain the preloaded state of the bolts and contact between the components. Linear modal analysis was performed about this preloaded state. This produced a prediction of the linearized natural frequencies of the BARC that didn't depend on model updating. Similarly, the nonlinearity in the BARC was predicted using quasi-static modal analysis [8], which consists of applying static loads in the shape of a mode of interest in order to predict its amplitude dependent natural frequency and damping ratio. This was also performed before any nonlinear tests had been performed. Hence, the paper presents an idea of the predictions that might be obtained with these tools based only on the nominal design of the components. These predictions are then compared with the actual test measurements.

The following section details the finite element model that was created, the validation steps that were performed, and the linear and nonlinear results obtained. Then Section 3 discusses the manufacturing of the actual BARC and the linear and nonlinear tests that were performed. The FEM and test results are then compared and conclusions are presented.

Creating a Finite Element Model of the BARC

A 3D finite element model (FEM) of the BARC was created using Abaqus from the provided drawings. The joints were modeled by creating simplified 3D bolts that were meshed with solid elements, as was found to work well in [2] as well as in the authors' prior work [9, 10]. The structure was preloaded by applying a bolt load in Abaqus to the middle surface of each bolt (see Figure 1) and then fixing the bolt length in the subsequent step. The specified torque values were converted to preload values using the plot of preload force versus torque found by Wall et al. in [11]. Furthermore, in [10] the best agreement with measurements was found when using a friction coefficient of 0.2, so this was used in Abaqus even though this is a lower value than typically expected for steel-on-steel contact.

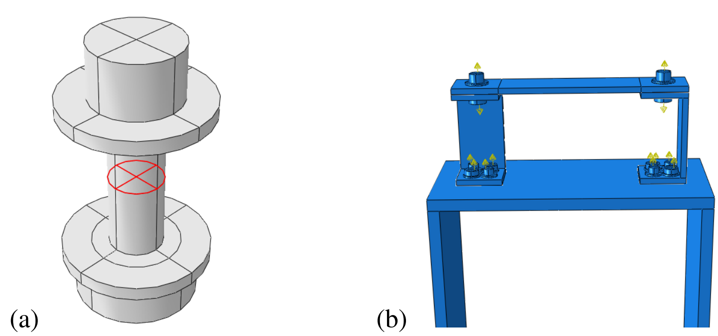

Fig. 1 (a) The surface that the bolt load is applied to is highlighted in red. (b) Yellow arrows represent the applied preload to those surfaces of each bolt.

The regions where contact was defined are shown in Figure 2. Notice that the interfaces between the bolts and the respective parts are tied in Abaqus instead of having contact defined because Jewell et al. [9] found these regions to contribute a negligible amount of damping and nonlinearity when similar joints were in a state of microslip.

The model was meshed with 3D, 8 node linear brick elements with reduced integration (C3D8R in Abaqus). In order to reduce the number of nodes in the model a separate part in Abaqus was created for the contact region on the box and is shown in Figure 4. These parts were then bonded together using a tie in Abaqus.

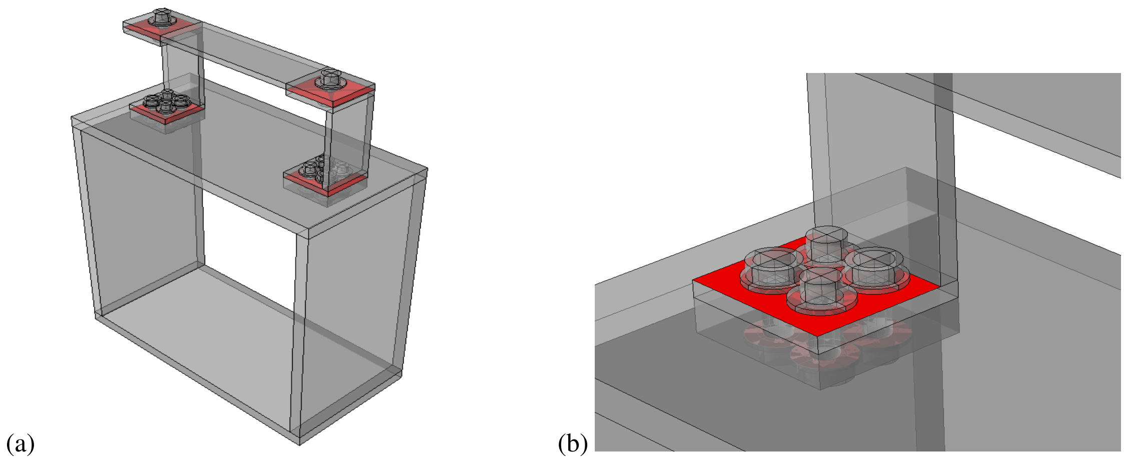

Fig. 2 (a) surfaces where contact was defined and (b) example of where a tie was used between the bolt heads and their mating surface.

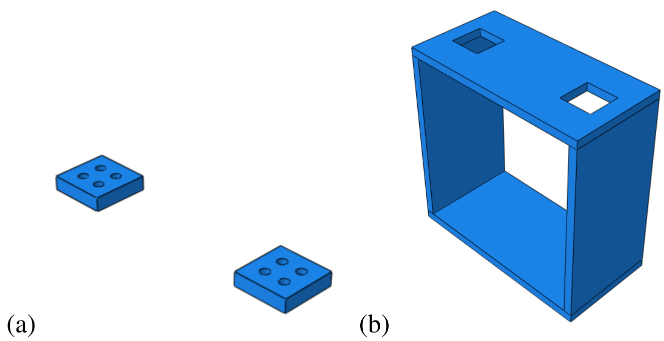

Fig. 3 (a) Separate parts created for the contact region, which had a fine mesh so that the contact could be resolved. (b) Remaining part of the box assembly, which had a coarser mesh. The parts shown in (a) were connected to the box using tie constraints.

Splitting the box into three parts as shown allows one to use a coarser mesh on the box without losing the ability to mesh the contact region finely so that contact at the interface could be resolved. This technique brought the number of nodes from $\approx$ 218,000 in our initial model to $\approx$ 110,000, essentially cutting the size of the model in half. These models are denoted the 218k model and the 110k model respectively in the following. To verify this technique, modal analysis was performed on both models and the natural frequencies of the first ten elastic modes were compared. The maximum and average errors were 3.24% and 2.05% respectively between the two models. This confirmed that the two models were acceptably similar while also minimizing the number of nodes. The authors also created a third model, called the 190k model, which had a similar density of elements as the 110k model over the box, but a much finer mesh over the contact region. The 218k model was used to compute the linear natural frequencies and mode shapes in all results below, because that computation was fast with either model. In the following subsection the results of quasi-static modal analysis are shown for these models and the computational savings are discussed.

Abaqus then solved for the linear mode shapes and natural frequencies of the preloaded structure with free-free boundary conditions. Figure 4 shows the first ten resulting mode shapes and natural frequencies. The results were compared to [5, 12] and found to agree reasonably well with their published natural frequencies and mode shapes.

Nonlinear Predictions from the FEM

Once the authors were comfortable that the model was giving accurate results, the mode shapes were examined to determine which might induce the most slip in the joints and hence the most nonlinearity. Mode 2 was chosen as the first promising candidate because vibration in that mode shears the RC. Quasi-static modal analysis (QSMA) [8] was applied to the FEM

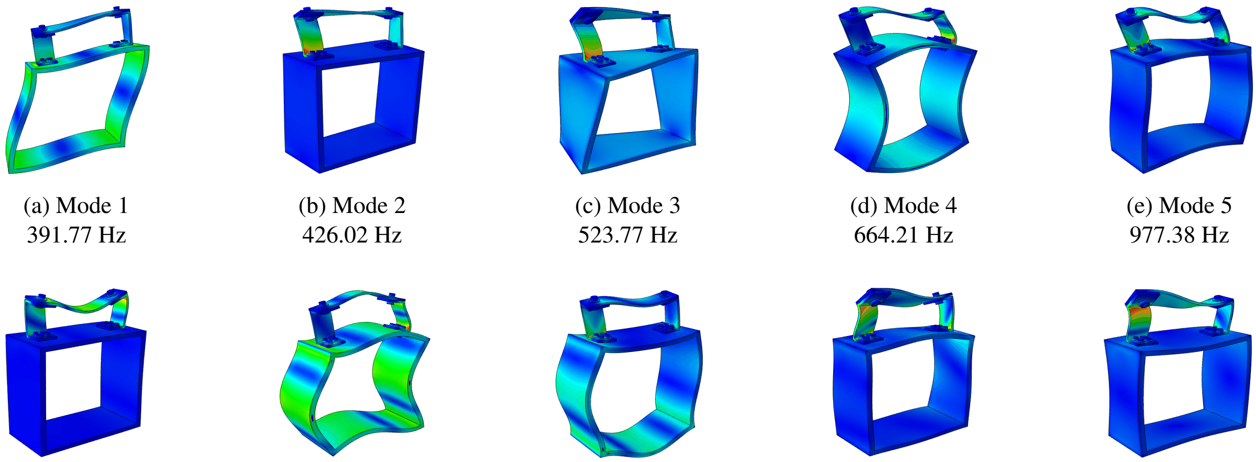

(a) Mode 1 391.77 Hz
(b) Mode 2 426.02 Hz
(c) Mode 3 523.77 Hz
(d) Mode 4 664.21 Hz
(e) Mode 5 977.38 Hz
(f) Mode 6 1072.9 Hz
(g) Mode 7 1359.7 Hz
(h) Mode 8 1516 Hz
(i) Mode 9 1655 Hz
(j) Mode 10 1699 Hz

Fig. 4 First ten elastic modes of the BARC and their natural frequencies in Hz

to predict the nonlinearity in this mode. QSMA is performed by applying a force in the shape of the mode of interest, and solving for the nonlinear static response of the structure when subjected to that force. The static load displacement curve can then be used to compute the effective damping and natural frequency. Details on the QSMA process can be found in [8]. The predictions from QSMA were obtained before any test data was available. Section presents the test results, which reveal which modes actually exhibited the most nonlinearity.

Figure 5 shows the damping versus amplitude and natural frequency versus amplitude curves obtained for Mode 2 using the 218k model. The process was repeated four times, with the force scaled to four different amplitudes, denoted by the

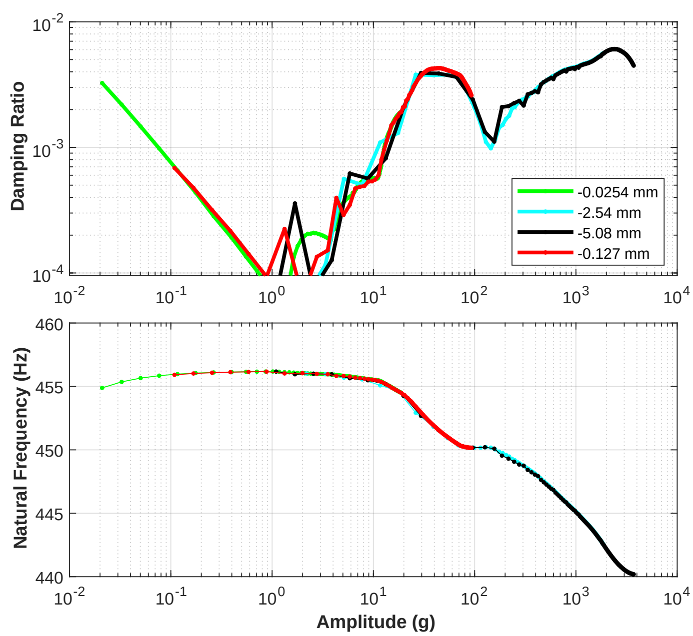

Fig. 5 Damping and Frequency vs. Amplitude for Mode 2. Each line represents a computation up to s different maximum force. These results are for the 218k model.

maximum displacement that each force would produce for the linear structure. These values ranged from 0.0254mm (0.001 in) to 5.08mm (0.2 in). The fact that the four curves agree with each other helps to verify that the behavior is physical and not an artefact of the numerical solution or function of the contact settings [9].

Figure 5 shows an increase in damping with amplitude as well as a decrease in frequency with amplitude. The damping increases with amplitude, up to a maximum value of about $\zeta = 0.005$, while the natural frequency decreases by about 15 Hz (3.3%). One would expect to be able to detect this level of damping and stiffness nonlinearity in a test. The QSMA predictions below about 1.0g are noisy, presumably because the mesh isn't fine enough to smoothly resolve the stick and slip transitions at this amplitude, so these should be ignored. At low amplitudes material damping would dominate so predictions are not needed for low amplitudes. At higher amplitudes the FEM shows microslip in the joints, which would likely be the source of the increase in damping observed here. Figure 7 shows the changing contact area and the slip in the joints as the analysis progresses. The mesh seems to be adequate to resolve a gradual change in the contact area and the sticking and slipping regions, providing additional confidence in the predictions.

Figure 6 compares the results between the 218k and 110k models. Although there is a shift in the frequency the trends between the two match well which helps validate this modeling technique. The 218k model, which had a single part for the box, took approximately 5.5 hours for the entire QSMA process while the 110k model, which had separate parts for the contact regions, finished in just under 3 hours. The fact that the results match suggests that one can reduce the computation time while keeping accuracy when examining a contact interface. This is especially helpful when one needs to run the model many times, for example to examine nonlinearity in several modes, or to cover a wide range of amplitude for a single mode. The frequency and damping for the 190k model were also nearly identical to these, so they were not shown here for brevity. The contact status for the 190k model was shown in Figure 7, where one can see that the overall areas of slip and stick were similar between the two models.

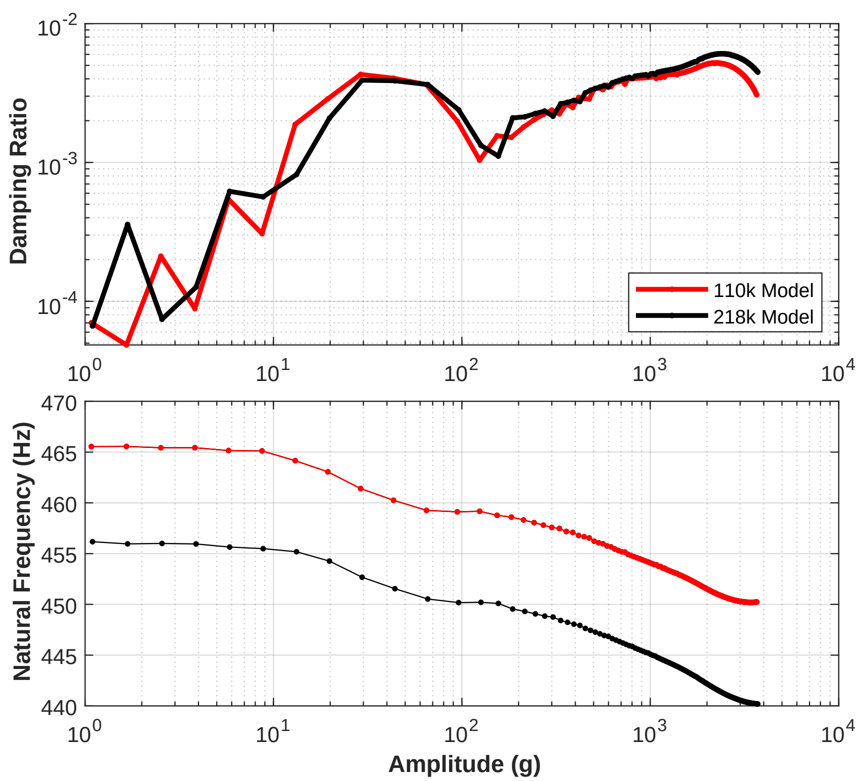

Fig. 6 Damping and Frequency vs. Amplitude for mode 2. The red line is from the 110k model and the black line is from the 218k model.

The authors also suspected that Mode 6 might exhibit nonlinearity, as the deformation of the removable component tends to want to open and close the bolted joints when the structure vibrates in that mode. QSMA was also attempted on this mode. Force displacement curves were obtained for a force applied in the shape of Mode 6 in both the positive and negative directions (i.e. a force that drives the removable component upward and downward respectively). These curves were compared and found to be significantly different. As a result, the standard QSMA approach could not be used on this

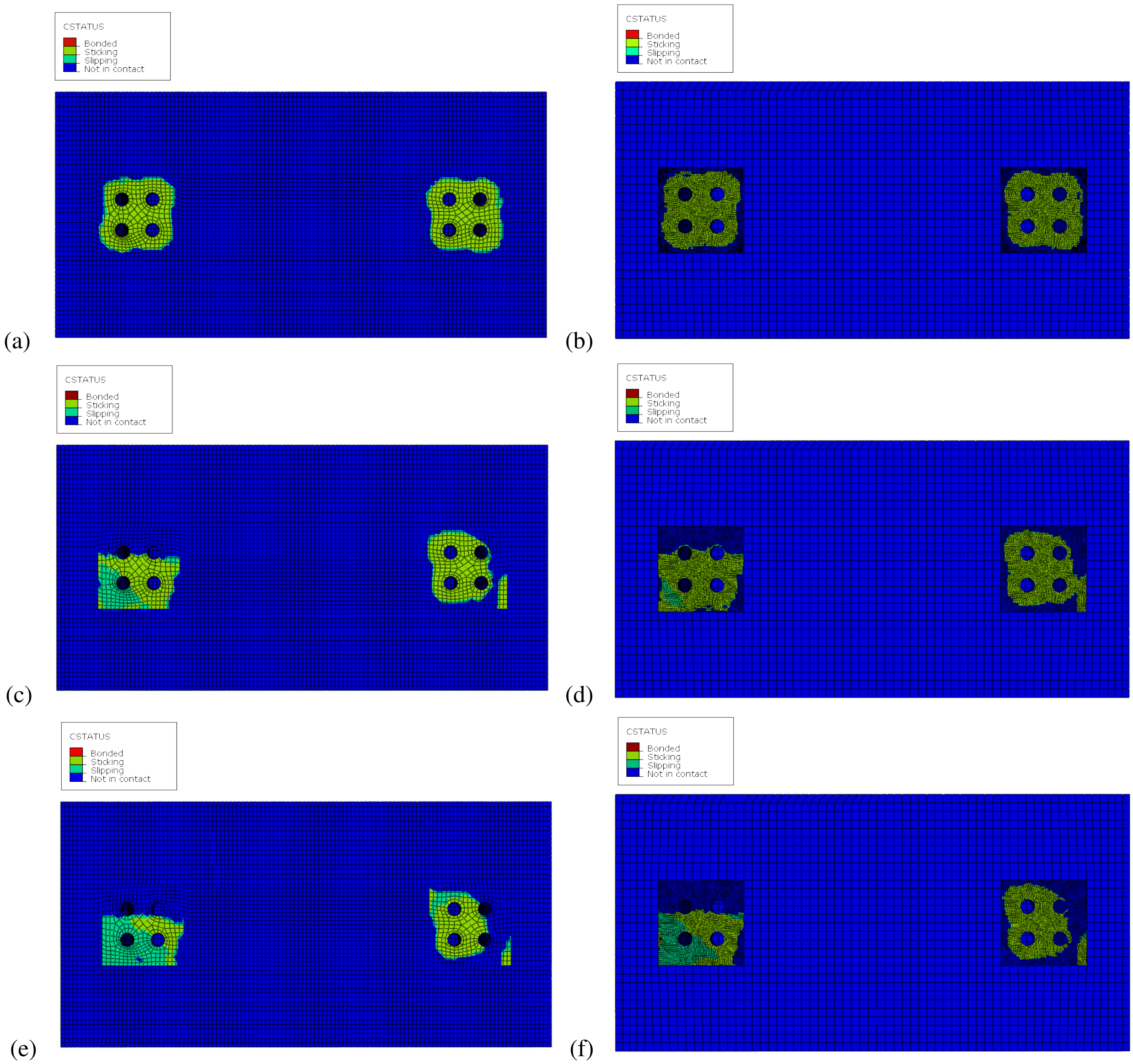

Fig. 7 The slip or stick status of the contact region on the box. (a), (c) and (e) show the 218k model, which has $\approx$ 5,600 nodes in the contact region while (b), (d) and (f) show the 190k model, which has $\approx$ 44,600 nodes on the contact region. (a) and (b) show the status at the beginning ($\approx$ 1g), (c) and (d) the middle ($\approx$ 500g), and (e) and (f) at the end ($\approx$ 4000g) of the QSMA analysis.

mode. One could instead use the approach developed by Shetty et al. [13], but time did now allow the authors to pursue this. instead it was simply noted that, based on the QSMA results, this mode might be expected to exhibit a bilinear-type nonlinearity.

Physical Testing

The BARC structure was manufactured per the drawings and instructions available on the Sandia website, which is in the process of being transitioned to another site hosted by SEM. A few of the washers had to be ground slightly so they wouldn't interfere when everything was assembled, but otherwise the structure was built per the drawings and reasonable tolerances seemed to have been achieved.

Linear Testing and Data Analysis

The BARC structure was hung from a metal frame by looping rope through the box component, then connecting the rope to 0.125 inch bungee cord, which then attached to the frame. Accelerometers were attached to several points, denoted $131Z+$, $133Z+$, $135Z+$, $231X-$, $231Y-$, $231Z+$, and $237Y-$ and shown in Figure 8. Using a tiny PCB impact hammer, each point was hit 3 times and averaged to obtain the frequency response functions (FRF) between the hammer and all accelerometers. The CMIF for the set of FRFs that was obtained is shown in Figure 9, and confirms that each mode appears at a distinct frequency in the spectrum.

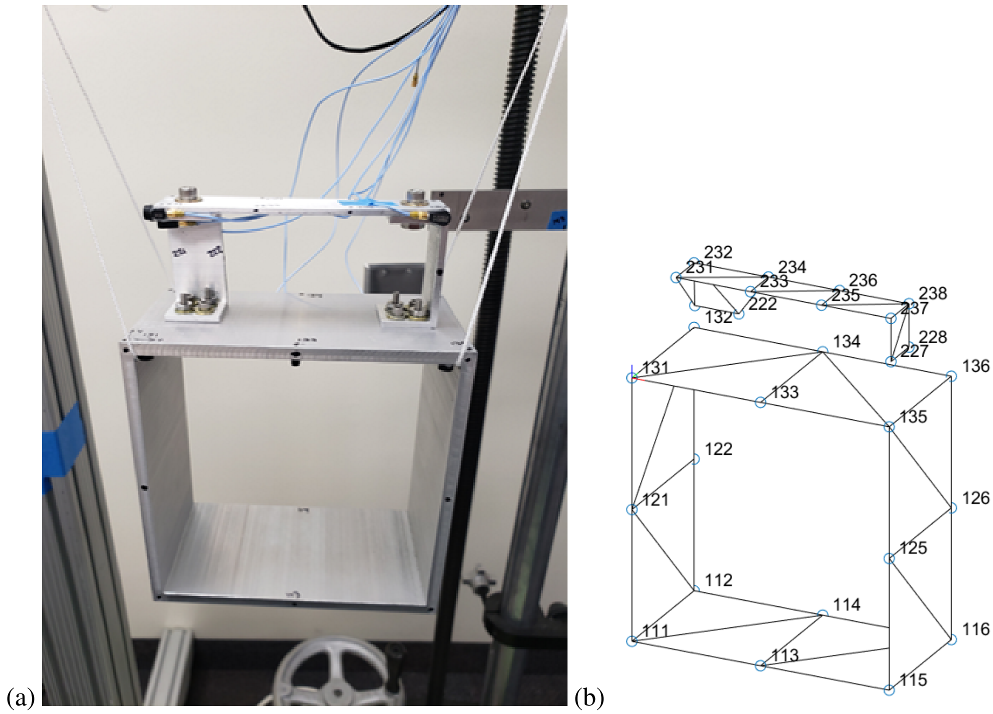

Fig. 8 (a) Photo of test setup for the BARC structure and (b) Measurement Grid

The set of FRFs was curve fit using the Algorithm of Mode Isolation and the modes below 2kHz were extracted. These are shown in Figure 10.

Nonlinear Testing and Data Analysis

A series of impacts was performed and the measurements processed to detect and characterize the nonlinearity in each of the first six modes. Based on the mode shapes shown in Figure 10, points for testing were chosen based on where the greatest displacement of the removable component was. A medium-sized hammer (PCB 086-C0x) was used for all modes except Mode 3. For that mode both a medium and large (PCB O86-D0x) hammers were used. Hence, the excitation location should have been that which best excites each mode. Data was processed in MATLAB using the Hilbert Transform as outlined in [14], which estimates the natural frequency and damping ratio as a function of vibration amplitude. The curves from various impacts were then combined into a single graph to check consistency.

Mode 1 responds in both the X and Z directions, and so impacts were applied in both directions. Figure 11 shows natural frequency and damping that were obtained from each of various impacts. The legend gives the impact number, maximum force, and the location and direction of the impact ($237X-$,$238X-$ or $231Z-$). The response was measured at point $231X-$ for X-direction hits and $231Z-$ for Z-direction hits. The amplitude on the x-axis is that of the acceleration at that point, which should be close to the maximum acceleration for the mode in question. Both sets of measurements show minimal change in the damping ratio, as the impact with the greatest damping ratio range (impact 28) only has a net change in damping of 0.08%. The natural frequency also shows a small change with amplitude. The results are similar for the Z-direction in Figure 11(b), although these results seem to show a sudden decrease in the natural frequency at higher amplitudes. The Z-direction measurements were taken on two different days, and it is interesting to note that the linear

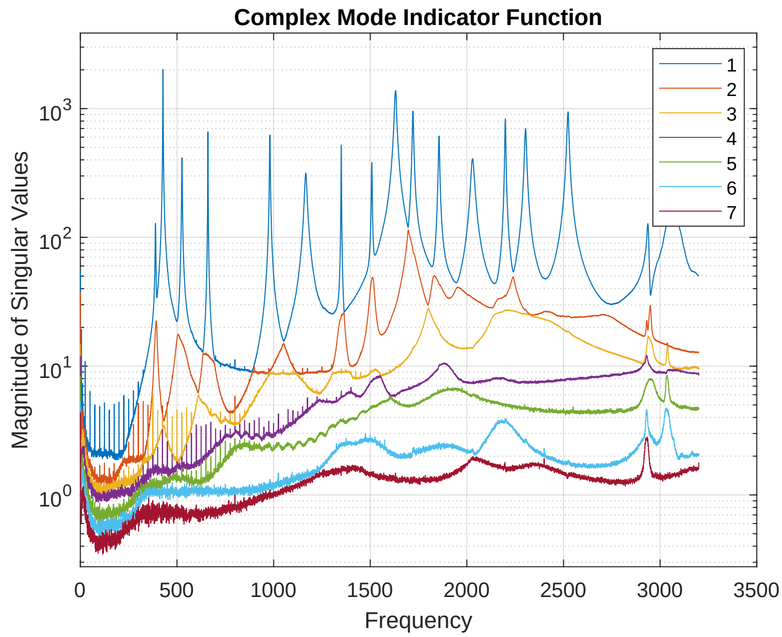

Fig. 9 Complex Mode Indicator Function for FRFs obtained in the linear test of the BARC

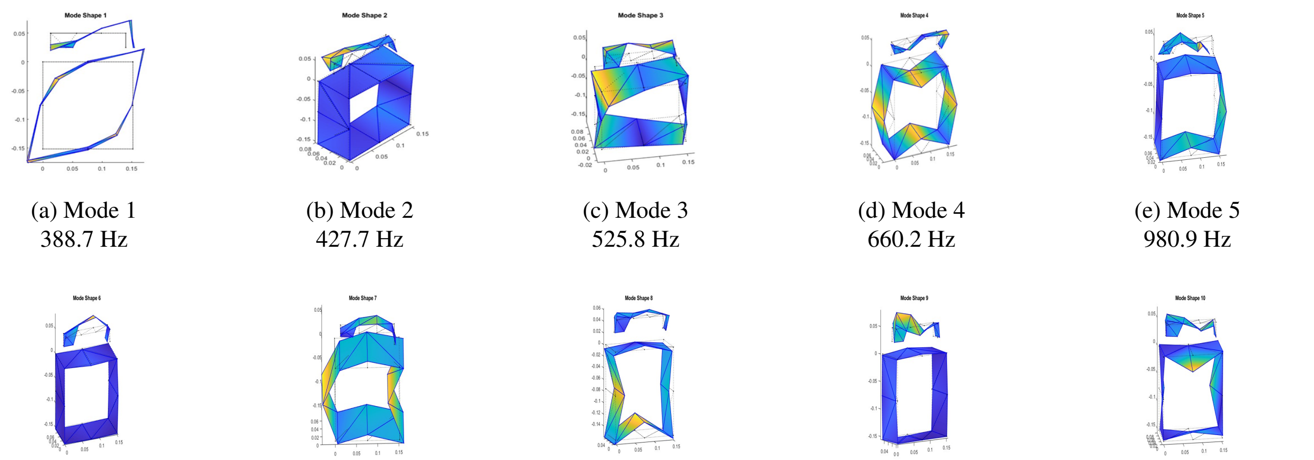

(a) Mode 1
388.7 Hz

(b) Mode 2
427.7 Hz

(c) Mode 3
525.8 Hz

(d) Mode 4
660.2 Hz

(e) Mode 5
980.9 Hz

(f) Mode 6
1166.8 Hz

(g) Mode 7
1350 Hz

(h) Mode 8
1508.2 Hz

(i) Mode 9
1631.6

(j) Mode 10
1721.1 Hz

Fig. 10 First ten elastic modes of the BARC and their natural frequencies in Hz

natural frequency appears to have shifted by about 0.2 Hz from one day to the next. In summary, Mode 1 a slight softening (stiffness) nonlinearity, yet it is small relative to experimental uncertainty.

Data for Mode 2 was taken on two separate days, 6/4/2024 and 6/7/2024, and as was the case for Mode 1, the linear natural frequency was slightly higher on the first day. The shift in the natural frequency is once again fairly small, only about 1.5Hz or 0.3%, all data does show the same trend. The damping increases by a factor of three or four. Both of these observations agree perfectly with the typical nonlinearity that is exhibited by bolted joints, as seen in [14, 15].

Data for Mode 3 was all collected on the same day, but using both the medium hammer (denoted *mh*, purple-yellow lines) and the big hammer (denoted *bh*, green and blue lines) in Figure 13. This mode was active along the top of the removable component near the center, so points 233-236 were excited in the negative Z direction. The big hammer didn't seem to be

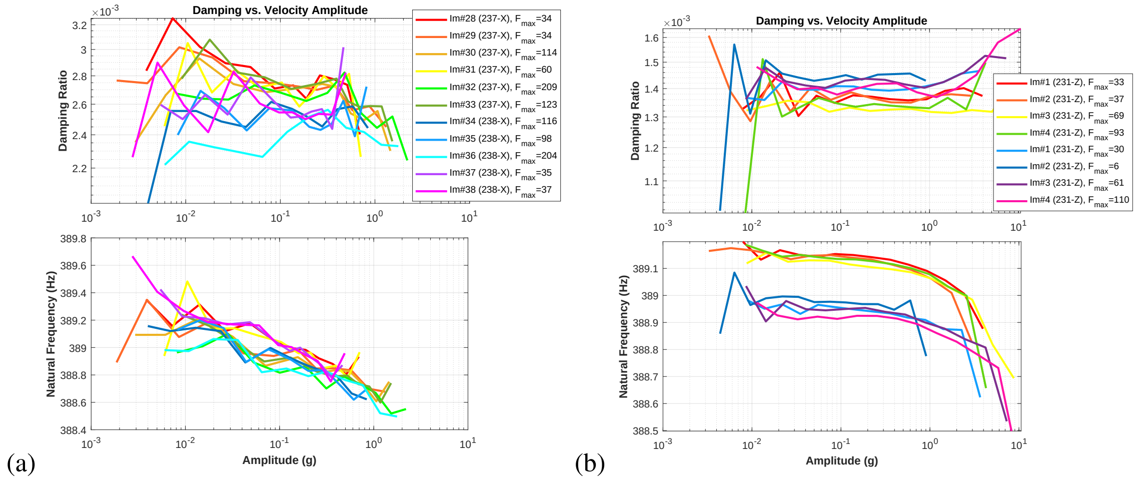

Fig. 11 Mode 1 Natural Frequency and Damping vs. Amplitude. The legend gives the impact number, maximum force, and the location and direction of the impact ($237X-$,$238X-$ or $231Z-$). Amplitude is that measured at points $231X-$ and $231Z-$ respectively.

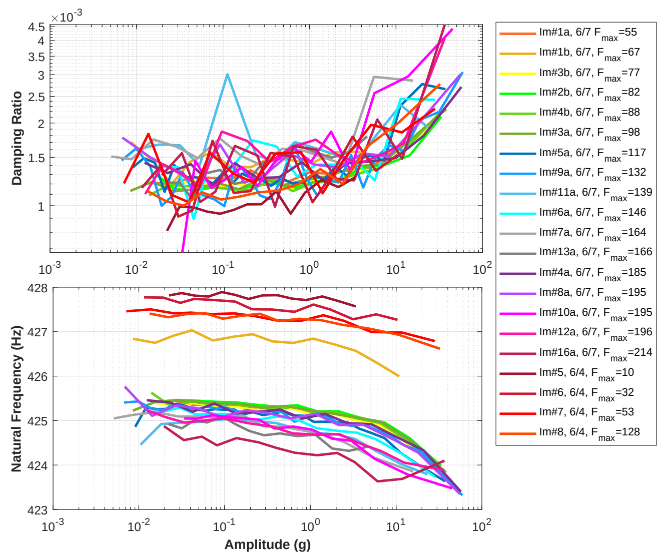

Fig. 12 Mode 2 Natural Frequency and Damping vs. Amplitude. All impacts were applied at $232Y-$ and amplitude is that measured at points $231Y-$.

able to excite any nonlinearity in this mode, as the measurements showed little to no change in the damping and natural frequency. The tip on that hammer may have been too soft to excite this mode effectively. The medium hammer did appear to produce changes at high amplitudes, the overall changes in the damping ratio (5e-4) and natural frequency (0.6 Hz or 0.2%) were fairly small.

Mode 4 was tested on 6/14/2024 (red-yellow lines) and 6/18/2024 (green-purple lines) at points 233 and 234 in the –Z direction. As with previous modes the linear natural frequencies were at slightly different values based on the day the data was taken, The damping shows no significant trend and while the frequency did decrease consistently on the second day of testing, the change was small (0.4 Hz or 0.06%).

Modes 5 and 6, shown in Figure 14, were somewhat difficult to process using the Hilbert Transform because they are somewhat close together and decayed quickly relative to the other modes. Hence, the results were somewhat noisy. Even then, the variation in these modes is small suggesting that they are behaving linearly.

To confirm that these modes were truly linear, the frequency response (FRF) was computed by dividing the FFT of the response by the FFT of the input force. The result, in Figure 15, shows that there is not a significant change in the stiffness

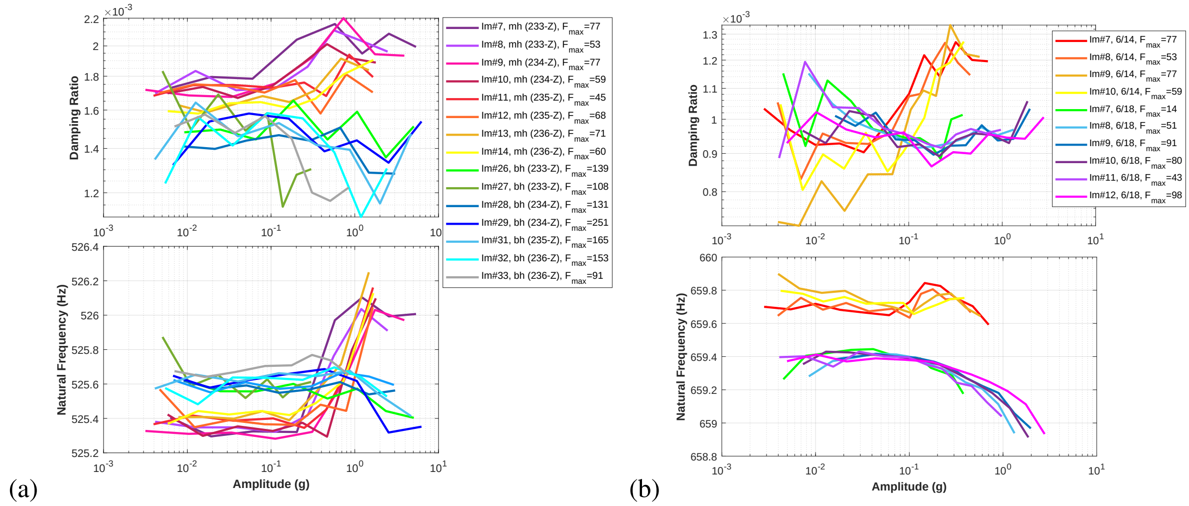

Fig. 13 (a) Mode 3 and (b) Mode 4 Natural Frequency and Damping vs. Amplitude. For Mode 4, impacts 9 and 10 were at $234Z-$ and all others were at $233Z-$. Amplitude is that measured at point $231Z-$.

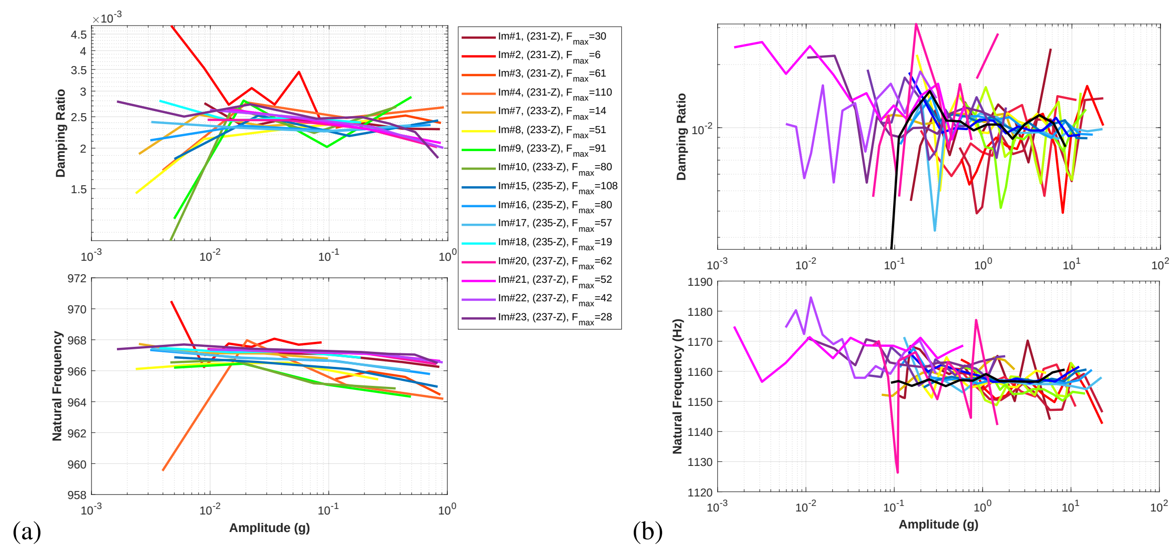

Fig. 14 (a) Mode 5 and (b) Mode 6 Natural Frequency and Damping vs. Amplitude. Amplitude is that measured at point $231Z-$.

or damping of these modes for the various impacts. Mode 5 does show an amplification of about 50% for Impact 17, as compared to the other tests, but the trend is not consistent for Impacts 18 and 19, which also had lower amplitudes.

Comparing Test Results and Predictions

Linear Mode Shapes and Natural Frequencies

The mode shapes, shown previously in Figures 4 and 10 show a strong visual correspondence between the FEM and test. These are repeated in Figures 17 and 18 in the Appendix to allow an easier comparison. The natural frequencies are compared in Table 1. They differed by at most 1.7% except for Mode 6, which differed by 8.0%. This is an opening-closing mode; the other modes don't involve this type of motion. Most of the natural frequencies agreed to within 1-2%.

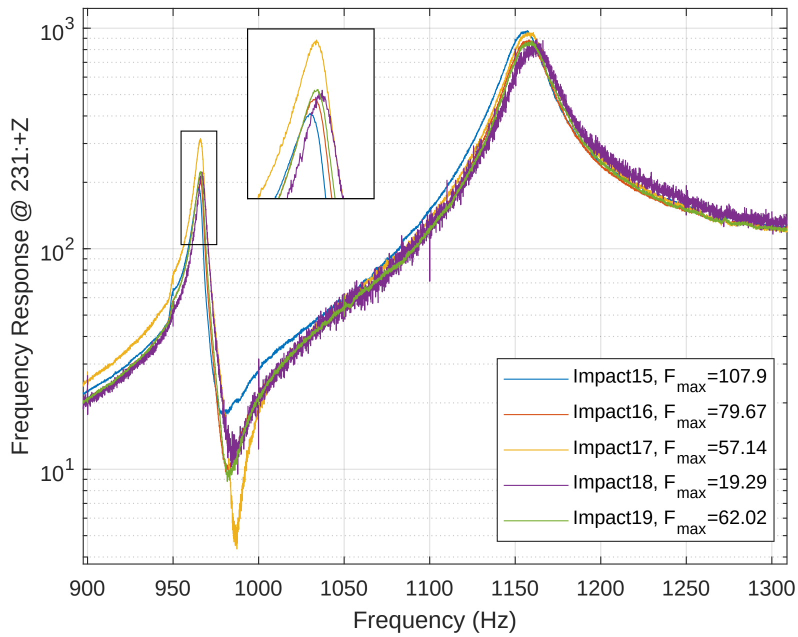

Fig. 15 Frequency Response Functions (FRFs) computed from several high amplitude impacts, to quantify nonlinearity in Modes 5 and 6.

Table 1 Comparison of Natural Frequencies between FEM and Test

Mode	FEM	Test	% Diff
1	391.77	388.7	0.79
2	426.02	427.7	-0.39
3	523.77	525.8	-0.39
4	664.21	660.2	0.61
5	977.38	980.9	-0.36
6	1072.9	1166.8	-8.0
7	1359.7	1350	0.72
8	1516	1508.2	0.52
9	1655	1629.3	1.6
10	1699	1721.1	-1.3

Nonlinearity

As was expected based on the FE analysis described in Section , Mode 2 showed the strongest nonlinearity in the test data. Furthermore, that mode exhibited a classical bolted-joint type nonlinearity, so one would expect QSMA to be effective at predicting its behavior. Figure 5 and 12 both show an increase in damping with amplitude as well as a decrease in frequency with amplitude. The damping also increases by a similar amount in both cases (about half an order of magnitude for a two-order of magnitude increase in vibration amplitude). These results are overlaid in Figure 16. To facilitate the comparison, material damping of $\zeta = 0.001$ was added to the FEM predictions, as this was clearly manifest in the test data. Note that the horizontal axis for the FEM data is the peak modal amplitude, or the product of the modal acceleration and the mode shape at the point where the displacement is largest. For the test data the horizontal axis is the acceleration amplitude at point $231Y-$, which appears to be the point of maximum displacement.

The FEM and Test results agree qualitatively, and have similar orders of magnitude. The anomaly in the damping that was observed in the FEM predictions around 3-6g happens to be the same region in which the test data shows the strongest nonlinearity; hence it would be wise to refine the model to make sure that the contact is well resolved for this amplitude. In contrast, if one extrapolates the power law behavior that the FEM exhibits from 200-2000g, that seems to agree with the lower bound of the test data. The lower bound is typically of interest in measurements such as this, as it

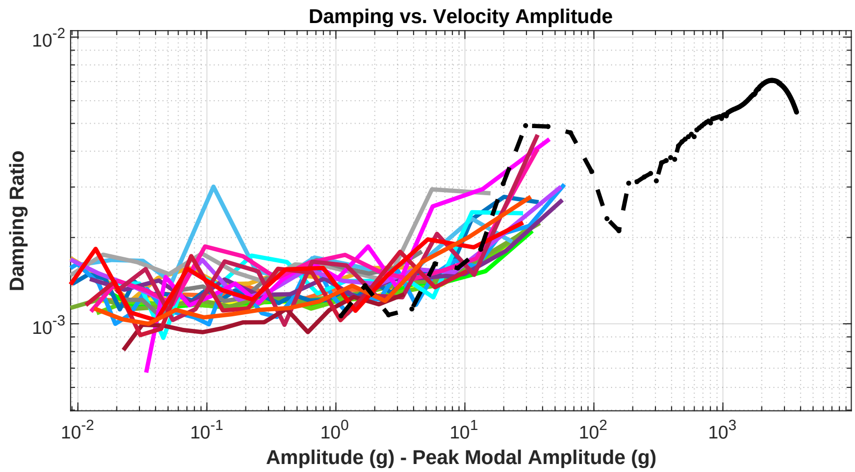

Fig. 16 Comparison of damping vs vibration amplitude between FEM and test for Mode 2: (black dashed) FEM Prediction, (colored lines) Measurements

would have the minimum influence from other modes (i.e. see [15]) and hence agrees best with the assumptions made in QSMA.

It is surprising that the results agree this well. In [10] the authors found that one had to model the interface very carefully, including any lack of flatness, to accurately capture damping.

The FEM analysis also noted that Mode 6 was likely to behave nonlinearly, with an opening-closing type nonlinearity. The measurements did not show significant nonlinearity in Mode 6. However, it should be noted that bilinear-type nonlinearities may not exhibit a significant change in the resonance frequency with vibration amplitude [16]. Further analysis would be required to see if the test data confirms any bilinear behavior of Mode 6.

Conclusion

The Box Assembly with Removable Component (BARC) was modeled using Abaqus FEA software in order to predict the linear mode shapes and natural frequencies. Then QSMA was performed on Mode 2, which was suspected to have nonlinear behavior, in order to predict the amplitude dependant damping ratio and natural frequency. These predictions from the FEM were complete before physical testing on the BARC structure was performed, thus giving blind predictions of the linear and nonlinear behavior based only on the nominal design of the components.

Once the FEM predictions were well along, the BARC was manufactured and linear and nonlinear testing was performed on the physical BARC structure. Modal analysis was performed in MATLAB to extract the linear mode shapes and natural frequencies. The mode shapes were found to visually match those of the FEM and the linearized natural frequencies from the FEM matched the tests well with typical errors of less than 1% and a maximum of 1.7% error, except for mode 6, which had an error of 8.0%. Mode 6 involves opening and closing of the joint while the other modes do not have this behavior. The first six modes were examined for nonlinearity and Mode 2 was found to exhibit a typical joint-type nonlinear damping behavior while the other modes had minimal nonlinearity. The nonlinearity predicted by applying QSMA on Mode 2 agreed quite well with the measurements.

This study demonstrates the feasibility of using finite element analysis and QSMA to predict the linear and nonlinear behavior of a component such as the BARC. The linear and nonlinear FEM predictions agreed very well with measurements in this study, but, as was cautioned earlier, research on other structures with joints [10] suggests that prediction may often be much more challenging. Still, these results are encouraging and motivate further use of these predictive tools.

Appendix

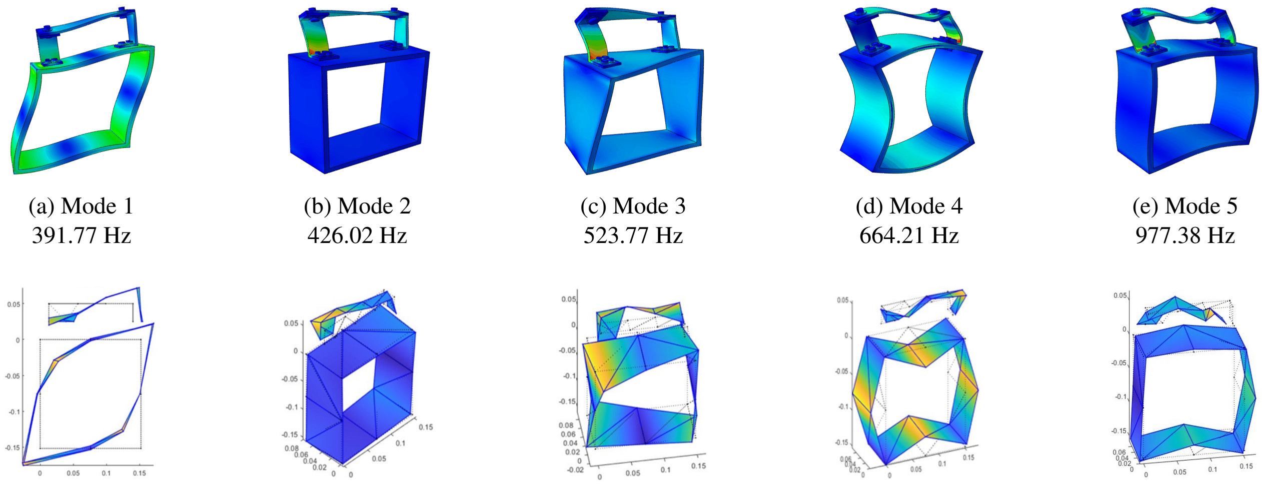

(a) Mode 1 391.77 Hz | (b) Mode 2 426.02 Hz | (c) Mode 3 523.77 Hz | (d) Mode 4 664.21 Hz | (e) Mode 5 977.38 Hz

(f) Mode 1 388.7 Hz | (g) Mode 2 427.7 Hz | (h) Mode 3 525.8 Hz | (i) Mode 4 660.2 Hz | (j) Mode 5 980.9 Hz

Fig. 17 Modes 1-5 with the FEM being on top and the mode shapes from tests on bottom.

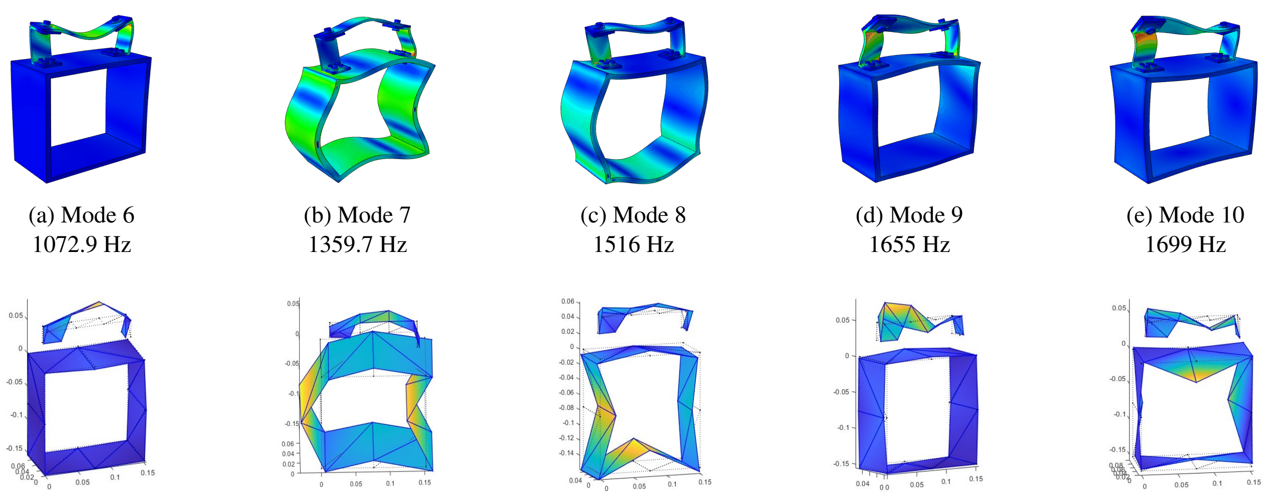

(a) Mode 6 1072.9 Hz | (b) Mode 7 1359.7 Hz | (c) Mode 8 1516 Hz | (d) Mode 9 1655 Hz | (e) Mode 10 1699 Hz

(f) Mode 6 1166.8 Hz | (g) Mode 7 1350 Hz | (h) Mode 8 1508.2 Hz | (i) Mode 9 1629.3 Hz | (j) Mode 10 1721.1 Hz

Fig. 18 Modes 6-10 with the FEM being on top and the mode shapes from tests on bottom.

References

1. David E. Soine, Richard J. Jones, Julie M. Harvie, Troy J. Skousen, and Tyler F. Schoenherr. Designing hardware for the boundary condition round robin challenge. In Michael Mains and Brandon J. Dilworth, editors, *Topics in Modal Analysis & Testing, Volume 9*, pages 119–126, Cham, 2019. Springer International Publishing.
2. Alvis, Tyler and Schoenherr, Tyler. Best Practices for Modeling Bolted Joints: Calibrating the BARC System. Orlando, FL, United states, February 2024.
3. Ryan Schultz, Tyler Schoenherr, and Brian Owens. A proposed standard random vibration environment for barc and the boundary condition challenge. In Chad Walber, Matthew Stefanski, and Steve Seidlitz, editors, *Sensors and Instrumentation, Aircraft/Aerospace, Energy Harvesting & Dynamic Environments Testing, Volume 7*, pages 77–84, Cham, 2022. Springer International Publishing.
4. Sebastian Chirinos, Aneesh Pawar, Haley Tholen, Scott Ouellette, and Thomas Roberts. Parametric simulations of the BARC model in SDOF and MIMO configurations for estimating service environment severity. In Chad Walber, Matthew Stefanski, and Julie Harvie, editors, *Sensors and Instrumentation, Aircraft/Aerospace and Dynamic Environments Testing, Volume 7*, pages 19–40. Springer International Publishing.
5. Christopher L. Padilla, Jonah M. Madrid, Ezekiel C. Granillo, Antonio Flores, and Abdessattar Abdelkefi. *Dynamics and nonlinear characterization of BARC systems with varying central cut widths*. American Institute of Aeronautics and Astronautics, Inc, 2024.
6. Ezekiel C. Granillo, Jonah M. Madrid, Christopher L. Padilla, Jorge Perez, and Abdessattar Abdelkefi. *Insights on the scalability of the BARC structure on its dynamical characteristics*. American Institute of Aeronautics and Astronautics, Inc, 2024.
7. Adam Takeshita. Experimental and computational investigations on fixture interference and accelerometer placement for barc systems. Master's thesis, New Mexico State University, Las Cruces, NM, USA, November 2022.
8. Robert M. Lacayo and Matthew S. Allen. Updating Structural Models Containing Nonlinear Iwan Joints Using Quasi-Static Modal Analysis. *Mechanical Systems and Signal Processing*, 118(1 March 2019):133–157, 2019. Number: 1 March 2019.
9. Emily Jewell, Matthew S. Allen, Iman Zare, and Mitchell Wall. Application of quasi-static modal analysis to a finite element model and experimental correlation. *Journal of Sound and Vibration*, 479(0022-460X):115376, 2020.
10. Seyed Iman Zare Estakhraji, Mitchell Wall, Jacob Capito, and Matthew S. Allen. A thorough comparison between measurements and predictions of the amplitude dependent natural frequencies and damping of a bolted structure. *Journal of Sound and Vibration*, 544:117397, February 2023.
11. Mitchell Wall, Matthew S. Allen, and Robert J. Kuether. Observations of modal coupling due to bolted joints in an experimental benchmark structure. *Mechanical Systems and Signal Processing*, 162(0888-3270):107968, 2022.
12. Daniel Peter Rohe. Modal data for the barc challenge problem test report. Technical Report SAND-2018-0640R; 660094, Sandia National Lab, 2018.
13. Drithi Shetty, Mathew S. Allen, and Kyusic Park. A New Approach to Model a System with Both Friction and Geometric Nonlinearity. *Journal of Sound and Vibration*, 522(26 May 2023):117631, 2023.
14. Daniel R. Roettgen and Matthew S. Allen. Nonlinear characterization of a bolted, industrial structure using a modal framework. *Mechanical Systems and Signal Processing*, 84:152–170, 2017.
15. Mitchell P. J. Wall, Allen Allen, Matthew S, and Robert J. Kuether. Observations of Modal Coupling due to Bolted Joints in an Experimental Benchmark Structure. *Mechanical Systems and Signal Processing*, 162:107968, 2022.
16. Benjamin R. Pacini, Wil A. Holzmann, and Randall L. Mayes. Performance of Nonlinear Modal Model in Predicting Complex Bilinear Stiffness. In Gaetan Kerschen, editor, *Nonlinear Dynamics, Volume 1*, Conference Proceedings of the Society for Experimental Mechanics Series, pages 101–112, Cham, 2019. Springer International Publishing.